



## The Formation of Massive Star Systems by Accretion

Mark R. Krumholz, *et al.*  
*Science* **323**, 754 (2009);  
DOI: 10.1126/science.1165857

**The following resources related to this article are available online at [www.sciencemag.org](http://www.sciencemag.org) (this information is current as of March 2, 2009):**

**Updated information and services**, including high-resolution figures, can be found in the online version of this article at:

<http://www.sciencemag.org/cgi/content/full/323/5915/754>

**Supporting Online Material** can be found at:

<http://www.sciencemag.org/cgi/content/full/1165857/DC1>

A list of selected additional articles on the Science Web sites **related to this article** can be found at:

<http://www.sciencemag.org/cgi/content/full/323/5915/754#related-content>

This article appears in the following **subject collections**:

Astronomy

<http://www.sciencemag.org/cgi/collection/astronomy>

Information about obtaining **reprints** of this article or about obtaining **permission to reproduce this article** in whole or in part can be found at:

<http://www.sciencemag.org/about/permissions.dtl>

# The Formation of Massive Star Systems by Accretion

Mark R. Krumholz,<sup>1\*</sup> Richard I. Klein,<sup>2,3</sup> Christopher F. McKee,<sup>2,4</sup>  
Stella S. R. Offner,<sup>4</sup> Andrew J. Cunningham<sup>3</sup>

Massive stars produce so much light that the radiation pressure they exert on the gas and dust around them is stronger than their gravitational attraction, a condition that has long been expected to prevent them from growing by accretion. We present three-dimensional radiation-hydrodynamic simulations of the collapse of a massive prestellar core and find that radiation pressure does not halt accretion. Instead, gravitational and Rayleigh-Taylor instabilities channel gas onto the star system through nonaxisymmetric disks and filaments that self-shield against radiation while allowing radiation to escape through optically thin bubbles. Gravitational instabilities cause the disk to fragment and form a massive companion to the primary star. Radiation pressure does not limit stellar masses, but the instabilities that allow accretion to continue lead to small multiple systems.

Stars can form with masses up to at least 120 times that of the Sun (1, 2), but the mechanism by which the most massive stars form is a long-standing mystery. Stars greater than  $\sim 20$  solar masses ( $M_{\odot}$ ) have Kelvin times (the time required for a star to radiate away its gravitational binding energy) that are shorter than their formation times, and as a result they attain their full luminosities while still accreting from their natal clouds. As the radiation from such an embedded, massive star diffuses outward through the dusty gas in the protostellar envelope, it exerts a force that opposes gravity. Spherically averaged, the ratio of the radiative and gravitational forces is  $7.7 \times 10^{-5} \kappa_0 (L/M)_{\odot}$ , where  $\kappa_0$  is the specific opacity of the gas in  $\text{cm}^2/\text{g}$  and  $(L/M)_{\odot}$  is the stellar light-to-mass ratio in units of  $L_{\odot}/M_{\odot}$  (where  $L_{\odot}$  is the luminosity of the Sun). Because the dusty envelopes of massive protostars have  $\kappa_0 \sim 5$ , the ratio of radiative to gravitational force exceeds unity for all stars with  $(L/M)_{\odot} \geq 2500$ . Main-sequence stars reach this value of  $(L/M)_{\odot}$  at masses of  $\sim 20 M_{\odot}$ . Therefore, radiation is expected to halt spherically symmetric infall (3, 4) near this mass. Two-dimensional simulations of massive star formation, which include rotation and thus an accretion disk that partially shields the gas from radiation (5, 6), find that radiation completely halts accretion once stars reach  $\sim 40 M_{\odot}$  (7); this is inconsistent with the highest known stellar masses.

Here, we report a three-dimensional simulation of the formation of stars with masses greater than  $20 M_{\odot}$  that includes the effects of radiation pressure. Three-dimensionality is important be-

cause instabilities that determine the interaction of gas and radiation, such as Rayleigh-Taylor instabilities, show faster growth rates and higher saturation amplitudes in three dimensions (8). Additionally, instabilities in accretion disks (9, 10) and the resulting formation of companion stars (11) can only be simulated when the disk is represented nonaxisymmetrically. It is important to consider these effects because most massive stars are members of multiple systems (12, 13).

Our initial conditions consisted of a gas cloud with mass =  $100 M_{\odot}$ , radius = 0.1 pc, and density profile  $\rho \propto r^{-1.5}$ , consistent with models (14, 15) and observations (16) of the initial states of massive prestellar cores. Its initial temperature was 20 K and it was in slow, solid-body rotation at a rate such that the ratio of rotational kinetic energy to gravitational binding energy was 0.02, which is consistent with the rotation rates seen in lower-mass cores (17). Previous two-dimensional simulations suggest that varying these parameters within the observed range of massive core properties would not alter the qualitative behavior (7). Even though observed massive cores have large turbulent velocities (16), we did not include turbulence in our initial conditions so as to focus on the effects of radiation pressure. Simulations that include the effects of turbulence (10) do not appear to produce qualitatively different results.

We evolved this initial state by means of our adaptive mesh refinement code ORION (18–22), which solves the equations of gravito-radiation-hydrodynamics in the gray, flux-limited diffusion approximation. The code dynamically increases resolution as needed down to a minimum cell size of 10 AU; regions that collapse to densities above the Jeans density at the maximum resolution become star particles, each of which produces a luminosity determined by a protostellar evolution model (23).

The simulation passed through several distinct phases (Fig. 1, figs. S1 to S3, and movie S1), forming multiple stars (Fig. 2). The cloud began

to collapse immediately and a central protostar formed 3600 years afterward. For the next 17,000 years, the protostar accreted smoothly via an axisymmetric disk (Fig. 1A). During this phase, the mass of the star grew to  $11 M_{\odot}$  and its luminosity remained below  $\sim 10^4 L_{\odot}$ . Because  $(L/M)_{\odot} < 1000$ , radiation pressure produced no noticeable effects. After  $\sim 20,000$  years, the disk became gravitationally unstable and developed a pronounced two-armed spiral that transported angular momentum efficiently (Fig. 1B) (24). Accretion onto the protostar continued smoothly.

Accretion, unimpeded by radiation pressure, continued until 25,000 to 26,000 years, when the star reached a mass of roughly  $17 M_{\odot}$  and achieved a sustained  $(L/M)_{\odot}$  value of  $\sim 2500$ , driven by Kelvin-Helmholtz contraction. This was luminous enough for its radiation pressure force to exceed the gravitational force, and the star began to drive gas outward around the polar axis, inflating radiation-filled bubbles both above and below the accretion disk (Fig. 1C). The density inside the bubbles was very low, and within them the radiation pressure exceeded the gas pressure by orders of magnitude. Almost all gas falling onto the protostar struck the walls of the bubbles, where it was shocked and swept up into the bubble walls. However, this did not slow accretion in our simulation, because the gas that struck the bubble walls eventually traveled along the margin until it reached the disk, at which point it continued to accrete onto the star. During this phase, radiation forces acting on material accreting onto the disk and gravitational forces acting on material in the disk caused it to become increasingly nonaxisymmetric. A series of small secondary stars formed in the disk, most of which advected inward because of dynamical friction with the gas and collided with the central protostar. As a result, the accretion rate onto the central star became variable, but its mean value remained roughly unchanged.

Around 35,000 years, a series of disk-borne stars collided and became massive enough to resist being dragged inward (Fig. 1D). The secondary star was initially smaller than the primary and orbited it, intercepting and accreting much of the inflowing gas (25). As a result, the secondary star acquired its own disk and grew faster at first than the primary, and the ratio of the mass of the secondary to that of the primary reached a value of  $>0.5$ . Thereafter, the disk continued to fragment but at a much-diminished rate, and accretion became almost evenly divided between the two massive stars. A third small disk-borne star was ejected into a wide orbit in our simulation, but eventually fell back and was captured and accreted. The total accretion rate onto the binary system varied periodically as the stars orbited one another, but its time-averaged value remained about the same as before binary formation. From this point onward, the bubbles showed instability and constantly changed shape while undergoing slow overall expansion. Accretion onto the system continued uninterrupted.

<sup>1</sup>Department of Astronomy, University of California, Santa Cruz, CA 95064, USA. <sup>2</sup>Department of Astronomy, University of California, Berkeley, CA 94720, USA. <sup>3</sup>AX Division, Lawrence Livermore National Laboratory, Livermore, CA 94550, USA. <sup>4</sup>Department of Physics, University of California, Berkeley, CA 94720, USA.

\*To whom correspondence should be addressed. E-mail: krumholz@ucolick.org

We halted the simulation at 57,000 years, after a  $\sim 20,000$ -year period when there was no further qualitative change in the evolution (Fig. 1E). At this point the system was a binary with a total mass of  $70.7 M_{\odot}$  and a time-averaged total luminosity of  $\sim 5 \times 10^5 L_{\odot}$ . The two stars had masses of  $41.5 M_{\odot}$  and  $29.2 M_{\odot}$  and were 1590 AU apart. Neglecting the effects of the gas, the semimajor axis of the orbit was 1280 AU (eccentricity 0.25), but because this neglects the gas, it may be an overestimate. Orbits like this are typical of young O stars, at least 40% of which are visual binaries with separations of  $\sim 1000$  AU (12). These are not the final system parameters, because the envelope and the disk still contained  $28.3 M_{\odot}$  of gas and the accretion rate had not diminished. However, the qualitative nature of the final system was well established.

We compared our result to two-dimensional simulations. The largest star that formed in any two-dimensional simulation with gray radiative transfer had a mass of  $22.9 M_{\odot}$ . If the simulation included a multifrequency treatment of the radiation, which we omitted because of its computational cost (23), the maximum mass of the star that formed was  $42.9 M_{\odot}$  (7). In these two-dimensional simulations, the initial phases of collapse, disk formation, and growth of a polar bubble were quite similar to ours, although the disk lacked nonaxisymmetric structure. In both cases there was a “flashlight effect” (7, 26) in which the disk beamed radiation preferentially in the polar direction. In two dimensions, however, as the star’s mass grew, radiation halted accretion over an ever larger fraction of the solid angle around the star. This eventually stopped infall onto the disk. Some of the gas remaining in the disk continued to accrete onto the star, but at a diminishing rate, and eventually the disk density became low enough for stellar radiation to blow it away.

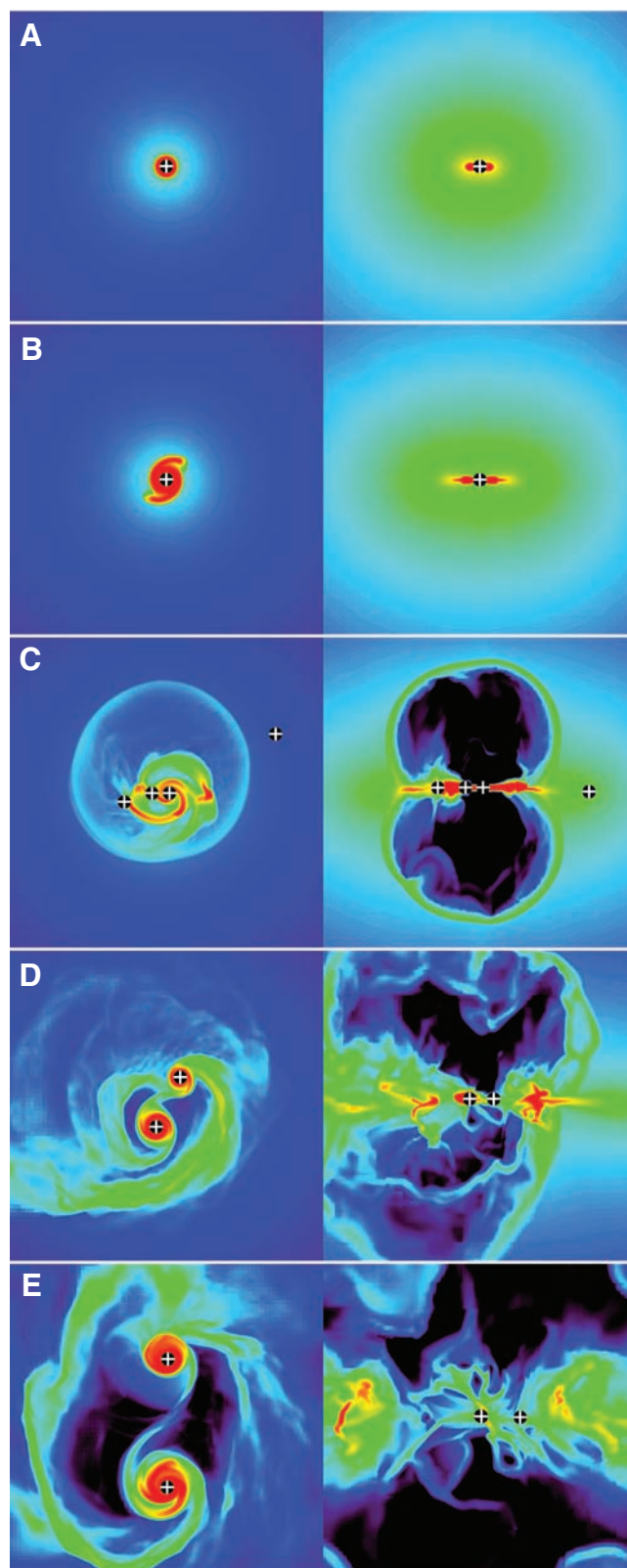
This never happened in our simulation. Instead, when the luminosity became large enough that our bubbles no longer delivered mass to the disk efficiently, they became asymmetric and clumpy. In some places radiation blew out sections of the bubble wall, whereas in others dense filaments of gas fell toward the stars (Fig. 3). The structure of dense fingers of heavy, downward-moving fluid alternating with chimneys of outgoing radiation is analogous to that of a classical Rayleigh-Taylor instability, with radiation taking the place of the light fluid. Radiation forces away from the star are stronger than gravity when averaged over  $4\pi$  sr, producing velocities and net forces that have an outward direction over most of the solid angle. Much of the mass is concentrated into the dense fingers, and because radiation flows around rather than through these structures, within them the velocity and the net force have an inward direction. However, this did not remove the angular momentum of the gas, so it continued to fall onto the disk rather than directly onto the stars. The growth of clumps in the disk that form secondary stars is a natural side effect of this process, but

radiation may be just accelerating a process that is caused by gravity. At least 40% of the accreting gas reached the disk through this Rayleigh-Taylor mechanism; gas falling onto the outer disk directly accounted for  $\sim 25\%$  of the accretion, and gas reaching the disk by traveling along the

bubbles’ outer walls contributed the remaining  $\sim 35\%$  (23).

Continued disk feeding is what made the three-dimensional results different from earlier two-dimensional ones. At 34,000 and 41,700 years (Fig. 1, C and D), bracketing the onset of

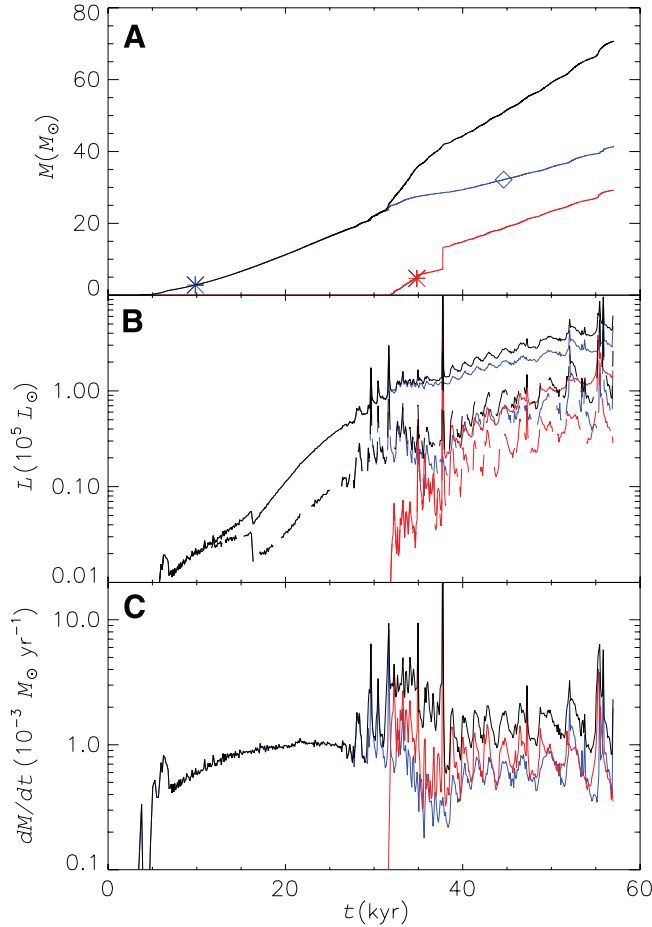
**Fig. 1.** Snapshots of the simulation at (A) 17,500 years, (B) 25,000 years, (C) 34,000 years, (D) 41,700 years, and (E) 55,900 years. In each panel, the left image shows column density perpendicular to the rotation axis in a  $(3000 \text{ AU})^2$  region; the right image shows volume density in a  $(3000 \text{ AU})^2$  slice along the rotation axis. The color scales are logarithmic (black at the minimum, red at the maximum), from  $10^0$  to  $10^{2.5} \text{ g cm}^{-2}$  on the left and  $10^{-18}$  to  $10^{-14} \text{ g cm}^{-3}$  on the right. Plus signs indicate the projected positions of stars. See Figs. S1 to S3 and movie S1 for additional images.



instability, the total stellar mass was  $32.4 M_{\odot}$  and  $46.9 M_{\odot}$ , respectively, and the disk mass was  $4.0$  to  $5.7 M_{\odot}$  and  $4.5$  to  $9.1 M_{\odot}$ , respectively. (The

range reflects the use of density cutoffs of  $10^{-14}$  to  $10^{-16} \text{ g cm}^{-3}$  to separate disk from nondisk material.) If accretion of gas onto the disk had

**Fig. 2.** (A) Stellar mass, (B) stellar luminosity, and (C) accretion rate as a function of time. Black lines show values summed over all stars, blue lines show values for the most massive star, and red lines show values for the second most massive star. In (A), asterisks mark the onset of deuterium burning and the diamond marks hydrogen burning. In (B), solid lines show luminosities from all sources (accretion, Kelvin-Helmholtz contraction, and nuclear burning); dashed lines show accretion luminosity only. Luminosities and accretion rates are 100-year running averages.



halted, then the evolution would likely have been the same as in the two-dimensional simulations. The remnant disk would still have accreted, but its low mass means that the stars would have gained less than  $10 M_{\odot}$  from it. In our three-dimensional simulation they instead accreted  $25$  to  $40 M_{\odot}$ , and did so at a constant rather than a declining accretion rate. Accretion of stars rather than gas did not contribute appreciably to this. The star with a final mass of  $\sim 40 M_{\odot}$  gained only  $1.8 M_{\odot}$  via collisions, whereas the  $\sim 30 M_{\odot}$  star gained  $1.2 M_{\odot}$ , excluding the initial collision that created it.

The final star formation efficiency for our simulated core was at least  $70\%$ , and a majority of the mass accreted within one mean-density free-fall time of the initial core ( $52,500$  years). Because infall was continuing at a roughly constant rate and no further qualitative changes were occurring at the time we halted the simulation, it is likely that much of the remaining mass would accrete onto the star system. In reality, protostellar outflows, which we have not included in our simulation, would limit the star formation efficiency to  $\sim 50\%$  (27, 28). Our result indicates that, relative to outflows, radiation pressure does not affect star formation efficiency or time scale. The cavities generated by outflows would reduce the effects of radiation pressure even further (29) and would modify the geometry of the radiation pressure bubbles or would prevent their formation altogether. Photon bubble instabilities, which can occur if the gas is sufficiently magnetized (30), might also reduce the effects of radiation pressure and modify the bubble geometry. Our simulation shows that even if these effects are omitted, radiation pressure does not present a barrier to massive star formation.

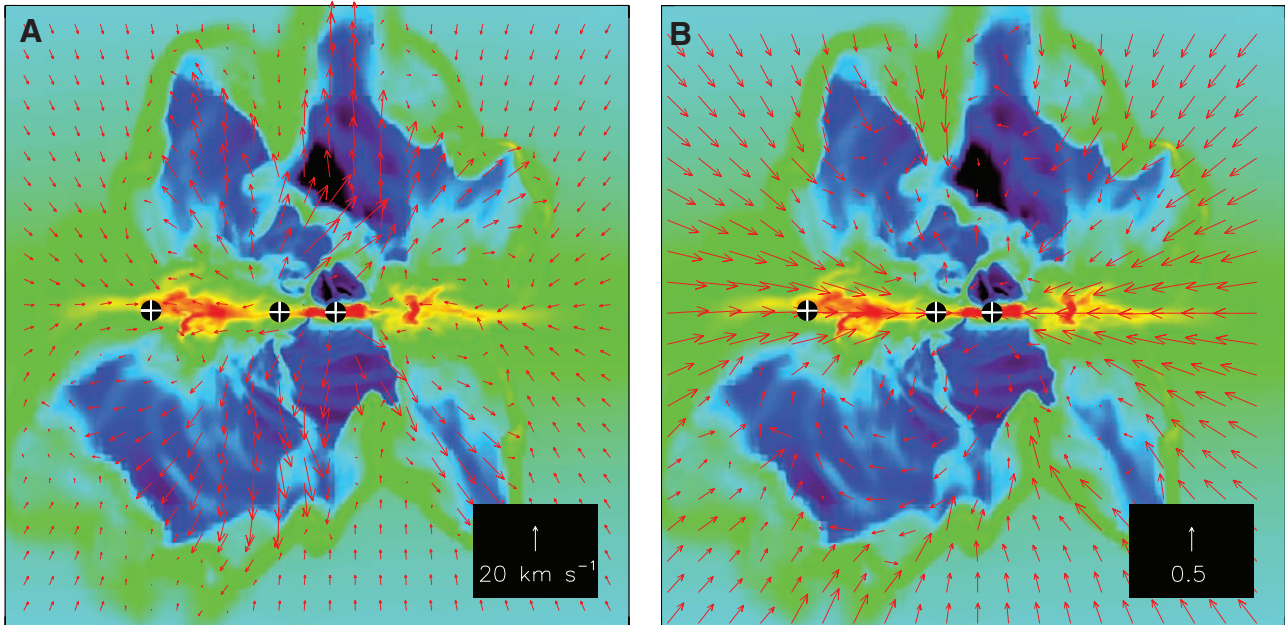


**Fig. 3.** Snapshot of a  $(6000 \text{ AU})^2$  slice along the rotation axis at  $51,100$  years. Color indicates density from  $10^{-20}$  to  $10^{-14} \text{ g cm}^{-3}$  on a logarithmic scale as in Fig. 1. Plus signs show projected stellar positions. (A) Arrows show gas velocity. (B) Arrow directions

indicate the direction of the net (radiation plus gravitational) force; lengths are proportional to the magnitude of the net force divided by the magnitude of the gravitational force. Thus, an inward arrow of length 1 represents negligible radiation force.

## References and Notes

- C. Weidner, P. Kroupa, *Mon. Not. R. Astron. Soc.* **348**, 187 (2004).
- D. F. Figer, *Nature* **434**, 192 (2005).
- F. D. Kahn, *Astron. Astrophys.* **37**, 149 (1974).
- M. G. Wolfire, J. P. Cassinelli, *Astrophys. J.* **319**, 850 (1987).
- T. Nakano, T. Hasegawa, C. Norman, *Astrophys. J.* **450**, 183 (1995).
- J. Jijina, F. C. Adams, *Astrophys. J.* **462**, 874 (1996).
- H. W. Yorke, C. Sonnhalter, *Astrophys. J.* **569**, 846 (2002).
- M. M. Marinak *et al.*, *Phys. Rev. Lett.* **75**, 3677 (1995).
- F. H. Shu, S. Tremaine, F. C. Adams, S. P. Ruden, *Astrophys. J.* **358**, 495 (1990).
- M. R. Krumholz, R. I. Klein, C. F. McKee, *Astrophys. J.* **656**, 959 (2007).
- K. M. Kratter, C. D. Matzner, M. R. Krumholz, *Astrophys. J.* **681**, 375 (2008).
- B. D. Mason *et al.*, *Astron. J.* **115**, 821 (1998).
- H. Sana, E. Gosset, Y. Nazé, G. Rauw, N. Linder, *Mon. Not. R. Astron. Soc.* **386**, 447 (2008).
- C. F. McKee, J. C. Tan, *Nature* **416**, 59 (2002).
- C. F. McKee, J. C. Tan, *Astrophys. J.* **585**, 850 (2003).
- H. Beuther *et al.*, *Astron. Astrophys.* **466**, 1065 (2007).
- A. A. Goodman, P. J. Benson, G. A. Fuller, P. C. Myers, *Astrophys. J.* **406**, 528 (1993).
- R. I. Klein, *J. Comput. Appl. Math.* **109**, 123 (1999).
- M. R. Krumholz, C. F. McKee, R. I. Klein, *Astrophys. J.* **611**, 399 (2004).
- R. T. Fisher, thesis, University of California, Berkeley (2002).
- M. R. Krumholz, R. I. Klein, C. F. McKee, J. Bolstad, *Astrophys. J.* **667**, 626 (2007).
- A. I. Shestakov, S. S. R. Offner, *J. Comput. Phys.* **227**, 2154 (2008).
- See supporting material on Science Online.
- G. Lodato, W. K. M. Rice, *Mon. Not. R. Astron. Soc.* **358**, 1489 (2005).
- M. R. Bate, *Mon. Not. R. Astron. Soc.* **314**, 33 (2000).
- H. W. Yorke, P. Bodenheimer, *Astrophys. J.* **525**, 330 (1999).
- C. D. Matzner, C. F. McKee, *Astrophys. J.* **545**, 364 (2000).
- J. Alves, M. Lombardi, C. J. Lada, *Astron. Astrophys.* **462**, L17 (2007).
- M. R. Krumholz, C. F. McKee, R. I. Klein, *Astrophys. J.* **618**, L33 (2005).
- N. J. Turner, E. Quataert, H. W. Yorke, *Astrophys. J.* **662**, 1052 (2007).
- Supported by NSF grants AST-0807739 (M.R.K.) and AST-0606831 (R.I.K. and C.F.M.); the Spitzer Space Telescope Theoretical Research Program, provided by NASA through a contract issued by the Jet Propulsion Laboratory (M.R.K.); NASA through Astrophysics Theory and Fundamental Physics Program grants NAG 05-12042 and NNG 06-GH96G (R.I.K. and C.F.M.); and the U.S. Department of Energy at Lawrence Livermore National Laboratory under contract B-542762 (R.I.K., S.S.R.O., and A.J.C.). This research used the Datastar system at the NSF San Diego Supercomputer Center (grant UCB267).

## Supporting Online Material

www.sciencemag.org/cgi/content/full/1165857/DC1

SOM Text

Figs. S1 to S5

Movie S1

References

12 September 2008; accepted 11 December 2008

Published online 15 January 2009;

10.1126/science.1165857

Include this information when citing this paper.

# Confined Crystallization of Polyethylene Oxide in Nanolayer Assemblies

Haopeng Wang,<sup>1</sup> Jong K. Keum,<sup>1</sup> Anne Hiltner,<sup>1\*</sup> Eric Baer,<sup>1</sup> Benny Freeman,<sup>2</sup> Artur Rozanski,<sup>3</sup> Andrzej Galeski<sup>3</sup>

The design and fabrication of ultrathin polymer layers are of increasing importance because of the rapid development of nanoscience and nanotechnology. Confined, two-dimensional crystallization of polymers presents challenges and opportunities due to the long-chain, covalently bonded nature of the macromolecule. Using an innovative layer-multiplying coextrusion process to obtain assemblies with thousands of polymer nanolayers, we discovered a morphology that emerges as confined polyethylene oxide (PEO) layers are made progressively thinner. When the thickness is confined to 20 nanometers, the PEO crystallizes as single, high-aspect-ratio lamellae that resemble single crystals. Unexpectedly, the crystallization habit imparts two orders of magnitude reduction in the gas permeability.

Crystalline polymers, such as polyethylene, polypropylene, poly(ethylene terephthalate), and nylon, have been broadly used as gas-barrier films in food, medicine, and electronics packaging, benefiting thereby from their low cost, easy processing, and mechanical toughness. Good barrier properties are imparted by the ability of polymer chains to crystallize into semi-crystalline materials with both crystalline and amorphous phases (1). The efficiency of chain packing is such that the crystalline phase is generally regarded as impermeable to even small gas molecules, and gas transport is seen as occurring through the amorphous regions (2). The processing conditions can be readily varied to control the amount of crystallinity and chain orientation and to tune the barrier properties of the final

product (3). With the growing use of polymers as thin and ultrathin films (4, 5), morphologies have been found resulting from constrained two-dimensional (2D) polymer crystallization (4, 6). These crystalline morphologies could possess gas permeability characteristics that are not expected from the bulk polymers.

Despite confinement, crystallization of polymer chains follows the conventional habit whereby polymer chains fold back and forth into stems to form crystalline lamellae with a thickness of ~10 to 20 nm. It is typical of crystallization from the isotropic melt that the lamellae are organized in a spherulitic morphology (7). However, the processes of nucleation and growth that control the crystallization kinetics can be profoundly affected by nanoscale confinement. The thickness of ultrathin polymer layers, usually a few tens of nanometers, is comparable to or a small multiple of the lamellar crystal thickness. Hence, the isotropic growth of lamellar crystals is greatly hampered, and crystallization under confinement can produce a specific lamellar crystal orientation. Often, the preferred lamellar crystal orientation is vertical to the layer (edge-on) (8, 9, 10). However, at the

other extreme, lamellar crystal orientation parallel to the layer (flat-on) is observed (6, 11–14). Although the mechanisms for the specific lamellar orientation during confined crystallization are still under investigation (15, 16), it is believed that the confined crystals will show anisotropic properties.

The 2D crystallization of polymers is conventionally studied with thin films or block copolymers that contain a crystallizable block. In the former, crystallizable layers with nanometer to submicron thicknesses are prepared by a solution process such as spin-coating (4, 17) or Langmuir-Blodgett (18) techniques. This approach is limited by the solvent requirement and by the small amount of material that can be fabricated. In the latter, a layered morphology on the nanometer scale is achieved as a consequence of microphase separation of the dissimilar blocks. If the crystallization temperature of the crystallizable block is below the order-disorder transition temperature (19), crystallization occurs with confinement in the layer-normal direction. A wide range of crystallizable blocks have been studied (8, 11–14, 16). However, elucidation of the structure-property relationships has been hindered by the need to synthesize the block copolymers and by the shear alignment that is required to construct the uniformly oriented phase structure (20).

In contrast to the self-assembled confinement created with microphase-separated block copolymers (21), layer-multiplying coextrusion uses forced assembly to create films with hundreds or thousands of alternating layers of two polymers (22, 23). Almost any melt-processable polymer can be fabricated into kilometers of nanolayered films, and layers less than 10 nm in thickness have been made. Although the amount of material in a single layer is very small, the properties of the confined layer are multiplied many-fold by the number of identical layers in the assembly. This enables us to use conventional methods to probe size-scale-dependent properties. Polyethylene oxide (PEO) was coextruded with poly

<sup>1</sup>Department of Macromolecular Science and Engineering, Case Western Reserve University, Cleveland, OH 44106–7202, USA. <sup>2</sup>Department of Chemical Engineering, University of Texas at Austin, Austin, TX 78758, USA. <sup>3</sup>Centre of Molecular and Macromolecular Studies, Polish Academy of Sciences, 90-363 Lodz, Poland.

\*To whom correspondence should be addressed. E-mail: ahiltner@case.edu